Astronomy & Astrophysics manuscript no. EGonzalez_GJ720A
March 18, 2021
©ESO 2021

arXiv:2103.09643v1 [astro-ph.EP] 17 Mar 2021

HADES RV Programme with HARPS-N at TNG

XIII. A sub-Neptune around the M dwarf GJ 720 A ⋆

E. González-Álvarez[1], A. Petralia[2], G. Micela[2], J. Maldonado[2], L. Affer[2], A. Maggio[2], E. Covino[3], M. Damasso[4], A. F. Lanza[5], M. Perger[6,7], M. Pinamonti[4], E. Poretti[8,9], G. Scandariato[5], A. Sozzetti[4], A. Bignamini[10], P. Giacobbe[4], G. Leto[5], I. Pagano[5], R. Zanmar Sánchez[5], J. I. González Hernández[11,12], R. Rebolo[11,12], I. Ribas[6,7], A. Suárez Mascareño[11,12], and B. Toledo-Padrón[11,12]

[1] Centro de Astrobiología (CSIC-INTA), Carretera de Ajalvir km 4, 28850 Torrejón de Ardoz, Madrid, Spain
[2] INAF-Osservatorio Astronomico di Palermo, Piazza Parlamento 1, 90134 Palermo, Italy
[3] INAF-Osservatorio Astronomico di Capodimonte, Salita Moiariello 16, 80131 Napoli, Italy
[4] INAF-Osservatorio Astrofisico di Torino, via Osservatorio 20, 10025 Pino Torinese, Italy
[5] INAF-Osservatorio Astrofisico di Catania, via S. Sofia 78, 95123 Catania, Italy
[6] Institut de Ciències de l'Espai (IEEC-CSIC), Campus UAB, Carrer de Can Magrans s/n, 08193, Bellaterra, Spain
[7] Institut d'Estudis Espacials de Catalunya (IEEC), 08034 Barcelona, Spain
[8] INAF-Osservatorio Astronomico di Brera, Via E. Bianchi 46, 23807 Merate, Italy
[9] Fundación Galileo Galilei – INAF, Rambla José Ana Fernandez Pérez 7, 38712 – Breña Baja, Spain
[10] INAF-Osservatorio Astronomico di Trieste, Via Tiepolo 11, 34143 Trieste, Italy
[11] Instituto de Astrofísica de Canarias, 38205 La Laguna, Tenerife, Spain
[12] Universidad de La Laguna, Dpto. Astrofísica, 38206 La Laguna, Tenerife, Spain

Received 3 February 2021 / Accepted 17 March 2021

ABSTRACT

Context. The high number of super-Earth and Earth-like planets in the habitable zone detected around M-dwarf stars in the last years has revealed these stellar objects to be the key for planetary radial velocity (RV) searches.
Aims. Using the HARPS-N spectrograph within The HArps-n red Dwarf Exoplanet Survey (HADES) we reach the precision needed to detect small planets with a few Earth masses using the spectroscopic radial velocity technique. HADES is mainly focused on the M-dwarf population of the northern hemisphere.
Methods. We obtained 138 HARPS-N RV measurements between 2013 May and 2020 September of GJ 720 A, classified as an M0.5 V star located at a distance of 15.56 pc. To characterize the stellar variability and to discern the periodic variation due to the Keplerian signals from those related to stellar activity, the HARPS-N spectroscopic activity indicators and the simultaneous photometric observations with the APACHE and EXORAP transit surveys were analyzed. We also took advantage of *TESS*, MEarth, and SuperWASP photometric surveys. The combined analysis of HARPS-N RVs and activity indicators let us to address the nature of the periodic signals. The final model and the orbital planetary parameters were obtained by fitting simultaneously the stellar variability and the Keplerian signal using a Gaussian process regression and following a Bayesian criterion.
Results. The HARPS-N RV periodic signals around 40 d and 100 d have counterparts at the same frequencies in HARPS-N activity indicators and photometric light curves. Then we attribute these periodicities to stellar activity the former period being likely associated with the stellar rotation. GJ 720 A shows the most significant signal at 19.466 ± 0.005 d with no counterparts in any stellar activity indices. We hence ascribe this RV signal, having a semiamplitude of 4.72 ± 0.27 ms^{-1}, to the presence of a sub-Neptune mass planet. The planet GJ 720 Ab has a minimum mass of 13.64 ± 0.79 $M_\oplus$, it is in circular orbit at 0.119 ± 0.002 AU from its parent star, and lies inside the inner boundary of the habitable zone around its parent star.

Key words. stars: late-type – stars: planetary systems – stars: individual: GJ 720 A

1. Introduction

Nowadays the high-precision spectrograph development has allowed to reach the necessary radial velocity (RV) precision to detect Neptune- and Earth-mass planets close and/or inside the habitable zone of late-type main-sequence stars. The M dwarf stars have turned out to be the ideal targets for detecting this type of planets (e.g., Tuomi et al. 2014; Dressing & Charbonneau 2015). The lower mass of the parent stars results in a higher Doppler RV amplitude for a given planetary mass than those for more massive stars. However, the M dwarfs tend to be active stars (Delfosse et al. 1998; Reiners et al. 2012) and it is known that the stellar activity hampers the detection of planets introducing periodic variations in the RV signals that mimic the signals with a Keplerian origin (Queloz et al. 2001; Robertson et al. 2014).

Send offprint requests to: E. González-Álvarez
egonzalez@cab.inta-csic.es

⋆ Based on observations collected at the Italian Telescopio Nazionale Galileo (TNG), operated on the island of La Palma by the Fundación Galileo Galilei of the INAF (Istituto Nazionale di Astrofisica) at the Spanish Observatorio del Roque de los Muchachos of the Instituto de Astrofísica de Canarias, in the framework of the HArps-n red Dwarf Exoplanet Survey (HADES).

Different approaches can be followed in order to disentangle the stellar activity signals from planetary induced signals. Spectroscopic activity indicators can be used to derive stellar activity variations and the stellar rotation period as well as simultaneous photometric and RV observations. The false frequencies analysis together with the coherence and the stability of the signals can also provide strong indications on the origin of the periodicity. A coherent and long-lived behaviour of the signal is expected in case the variations are caused by a Keplerian motion. The RV technique is affected by the contribution of both stellar activity and Keplerian modulations, therefore a model that considers simultaneously the stellar variability through the Gaussian Process (GP) regression together with a fit of the planetary orbital parameters can be crucial when determining the Keplerian parameters.

Here, we present the high-precision, high-resolution spectroscopic measurements of the M0.5V star GJ 720 A (HIP 91128, BD+45 2743) obtained with the HARPS-N spectrograph (Cosentino et al. 2012) on the Telescopio Nazionale *Galileo* (TNG) as part of the HArps-n red Dwarf Exoplanet Survey (HADES).

The HADES collaboration has already produced many valuable results, regarding the statistics, activity, and characterization of M stars (Perger et al. 2017; Maldonado et al. 2017; Scandariato et al. 2017; Suárez Mascareño et al. 2018; González-Álvarez et al. 2019), and has led to the discovery of several planets (Affer et al. 2016; Suárez Mascareño et al. 2017; Perger et al. 2017; Pinamonti et al. 2018; Affer et al. 2019).

In Section 2, we introduce the target star (GJ 720 A) and present the stellar properties, newly derived and collected from the literature. Section 3 presents the observations carried out including high-resolution spectroscopy and photometric variability monitoring. In Section 4, we provide a detailed analysis of the HARPS-N radial velocities, spectroscopic activity indicators, and photometric light curves with the main goal of determining the presence of planet candidates. The properties of the newly discovered planet orbiting GJ 720 A are given in Section 5. A brief discussion on the implications of this finding and the conclusions of this paper appear in Section 6.

2. GJ 720 A

GJ 720 A is an M0.5 V dwarf located at a distance of 15.557 ± 0.006 pc (Bailer-Jones et al. 2018) from the Sun. As published by Luyten (1979) GJ 720 A (LHS 3394) has a wide companion called GJ 720 B (other names: LHS 3395 and VB 9) with relative position measured since 1960. Following the most updated classification (Alonso-Floriano et al. 2015) GJ 720 B is an M2.5 V star and the projected separation between GJ 720 A and B is 112.138 arcsec.

In this work we focus on the primary star GJ 720 A, its basic stellar parameters (effective temperature, stellar metallicity, spectral type, mass, radius, surface gravity, and luminosity) were computed by using the same spectra used here in the RV analysis and following the procedure described in Maldonado et al. (2015) and Maldonado et al. (2017). The most updated stellar parameters of GJ 720 A collected from the literature are compiled in Table 1. During the guaranteed CARMENES exoplanet survey (Reiners et al. 2018) GJ 720 A was also observed as part of their M dwarf sample. The stellar parameters derived from the CARMENES spectra were published in Schweitzer et al. (2019). All of them agree, within the 1σ error bars, with those derived here using the HARPS-N spectra.

GJ 720 A is not a very active star and shows moderate chromospheric flux (Maldonado et al. 2017). This is consistent with the slow rotation of GJ 720 A, which has a projected rotational velocity $v \sin i = 0.99 \pm 0.53\,\mathrm{km\,s^{-1}}$ (Maldonado et al. 2017). GJ 720 A has been observed in X-rays by *ROSAT* and we derived its X-ray luminosity, $\log L_X = 27.26 \pm 0.15\,\mathrm{erg\,s^{-1}}$ (González-Álvarez et al. 2019). From its X-ray luminosity, the activity level is typically found among medium active stars of its spectral type. GJ 720 A has a rotation period (P_{rot}) of 34.5 ± 4.7 days determined from Ca II H & K and $H\alpha$ spectroscopy time-series in Suárez Mascareño et al. (2018). Also Giacobbe et al. (2020) confirms this value in the contex of the photometric analysis of APACHE survey data. The chemical composition analysis available reveals that GJ 720 A has a slightly sub-solar metallicity.

Table 1. Stellar parameters of GJ 720 A.

Parameters	Value	Ref.[a]
Other name	HIP 91128	
α (J2000)	18:35:19.08	*Gaia DR3*
δ (J2000)	+45:44:44.4	*Gaia DR3*
G (mag)	9.1050 ± 0.0005	*Gaia DR2*
J (mag)	6.88 ± 0.02	2MASS
Spectral type	M0.5 V	Mald17
π (mas)	64.236 ± 0.012	*Gaia DR3*
d (pc)	15.557 ± 0.006	*Bail18*
$\mu_\alpha \cos\delta$ (mas yr^{-1})	452.36 ± 0.01	*Gaia DR3*
μ_β (mas yr^{-1})	363.47 ± 0.01	*Gaia DR3*
From HARPS-N spectra		
$T_{\rm eff}$ (K)	3837 ± 69	*Mald17*
$\log g$ (cgs)	4.71 ± 0.05	*Mald17*
[Fe/H] (dex)	−0.14 ± 0.09	*Mald17*
M ($M_\odot$)	0.57 ± 0.06	*Mald17*
R ($R_\odot$)	0.56 ± 0.06	*Mald17*
$\log L_{\rm bol}/L_\odot$	−1.217 ± 0.0964	*Mald17*
$v \sin i$ (km s^{-1})	0.99 ± 0.53	*Mald17*
$\log R'_{\rm HK}$	−5.03 ± 0.04	*Suar18*
$P_{\rm rot}$ (days)$^{(*)}$	$36.05^{+1.38}_{-1.44}$	*This work*
$\log L_{\rm x}$ (erg s^{-1})	27.39 ± 0.15	*Gonz19*
$\log L_{\rm x}/L_{\rm bol}$	−5.11 ± 0.18	*Gonz19*

Notes. [(a)] *Gaia* DR3: Gaia Collaboration et al. (2020); *Gaia* DR2: Gaia Collaboration et al. (2018); 2MASS: Cutri et al. (2003); Mald17 : Maldonado et al. (2017); Bail18: Bailer-Jones et al. (2018); Gonz19: González-Álvarez et al. (2019); Suar18: Suárez Mascareño et al. (2018). [(*)] $P_{\rm rot}$ value derived from the S-index activity indicator.

3. Observations

3.1. HARPS-N radial velocities

GJ 720 A has been monitored from the 26th of May 2013 to the 1st of September 2020 for a total of 138 data points. Of the 138 HARPS-N epochs, 75 were obtained within the GAPS observing program and 63 within the Spanish observing program. The spectra were obtained with the high resolution (resolving power $R \sim 115,000$) optical echelle spectrograph HARPS-N. The exposure time was set to 15 minutes yielding an average signal-to-noise ratio (S/N) of 76 at 5500 Å. Data were reduced using the latest version of the Data Reduction Software (DRS V3.7, Lovis & Pepe 2007). For GJ 720 A the M2 mask was used. The RVs were computed by matching the spectra with a

high S/N template obtained by co-adding the spectra of the target, as implemented in the Java-based Template-Enhanced Radial velocity Re-analysis Application (TERRA, Anglada-Escudé & Butler 2012). TERRA provides more accurate RVs when it is applied to M dwarfs, considering orders redder than the 22nd. The GJ 720 A TERRA RVs show a root mean square (*rms*) dispersion of 4.19 m s^{-1} and a mean internal error of 0.9 m s^{-1}. The HARPS-N RV time-serie is shown in the top panel of Figure 1 while the RV data are provided in Table A.1.

The TERRA pipeline also provides measurements for a number of spectral features and other diagnostics of stellar activity (e.g., Ca II H & K (S-index), the Na I D line, and Hα). The derived values are given in Table A.1 and the corresponding time-series are shown in Figure 1.

3.2. Photometric time series

SuperWASP and MEarth. GJ 720 A was photometrically observed by the Wide Angle Search for Planets (SuperWASP) exoplanet transit survey (Smith & WASP Consortium 2014) and the MEarth (Berta et al. 2012) survey. There were three photometric campaigns using the MEarth telescopes between 2008 and 2010, from 2011 to 2014, and between 2011 and 2017. The first two campaigns were conducted in the Northern Hemisphere with a total number of datapoits of 632 (*rms* of 8.8 mmag) and 984 (*rms* of 6.9 mmag), respectively. While the last one was carried out in the South with 1,480 measurements (*rms* of 6.2 mmag). The original photometric data presented several outliers and we applied a 2.5σ-clipping algorithm to remove them. The outliers were also removed from the SuperWASP photometric data taken between 2004 and 2008. The different photometric time-series are presented if Fig. 2.

EXORAP. We monitored GJ 720 A also in the framework of the EXORAP project at the INAF-Catania Astrophysical Observatory with an 80 cm f/8 Ritchey-Chretien robotic telescope (APT2) located at Serra la Nave on Mt. Etna. We collected ~5 yr of B, V, R, and I-band photometry in order to obtain simultaneously photometric and spectroscopic data. We performed data reduction by applying overscan, bias, dark subtraction, and flat fielding with IRAF[1] procedures and visual inspection to check the image quality (see Affer et al. 2016 for details). Errors in the individual photometric points include the intrinsic noise (photon noise and sky noise) and the *rms* of the ensemble stars used for computing the differential photometry. The final dataset contains ~240 photometric points for each of the *B*, *V*, *R* and *I* bands distributed over 5 consecutive seasons, between MJD=56555 and MJD=58034 (*B* filter shown in Fig. 1).

APACHE. 44 of the HADES targets (including GJ 720 A) were also monitored photometrically by APACHE (A PAthway towards the CHaracterization of Habitable Earths) photometric transit search project (Sozzetti et al. 2013). Our target was very intensively observed by APACHE, having 163 nights over a timespan of 1250 days, for a total of 5900 points in the *V*-band. The APACHE photometric observing epochs (binned data are shown in Fig. 1) partially overlap with the spectroscopic observations carried out within HADES, therefore the photometric and spectroscopic activity data analyzed here are partially simultaneous.

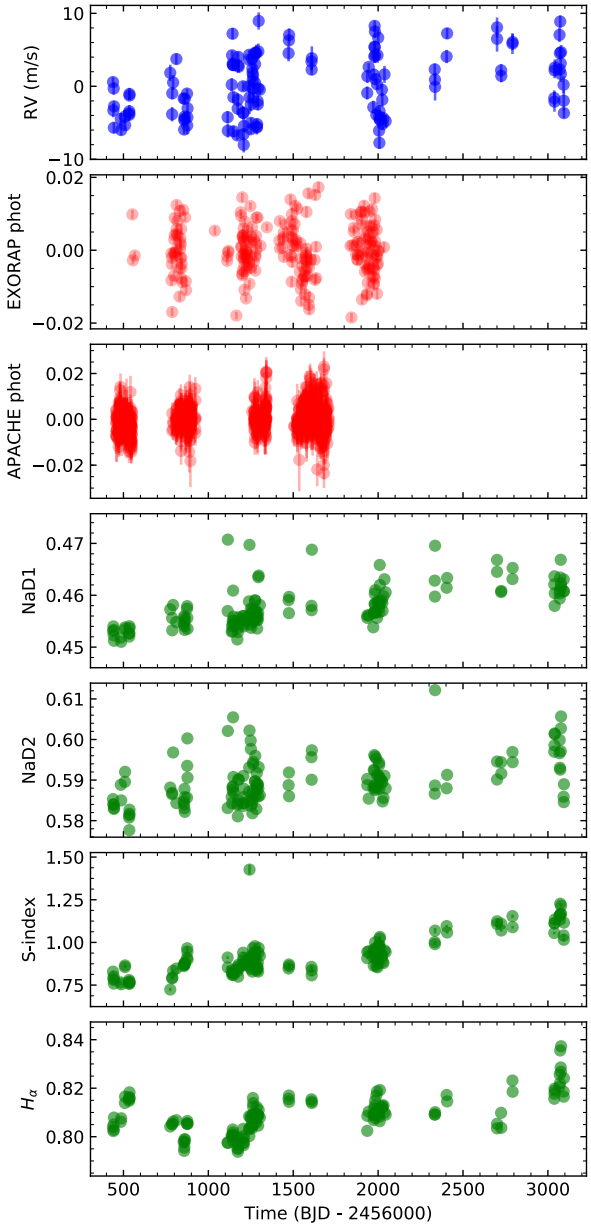

Fig. 1. Radial velocity (blue dots), EXORAP (*B*-band) and APACHE (*V*-band) photometric (red dots), and spectroscopic (green dots) activity indicators time-series for GJ 720 A.

TESS. GJ 720 A (TIC122958010) star was observed by *TESS* in sector 14 between 2019 July 18 and August 15 and in sector 26 between 2020 July 18 and August 15. The light curves and the target pixel (TPFs) files for the different sectors were downloaded from the Mikulski Archive for Space Telescopes (MAST) which is a NASA founded project. We verified the pixels in the aperture FITS extension and marked those that were used in the optimal photometric aperture in order to check that there is no

[1] IRAF is distributed by the National Optical Astronomy Observatories, which are operated by the Association of Universities for Research in Astronomy, Inc., under cooperative agreement with the National Science Foundation.

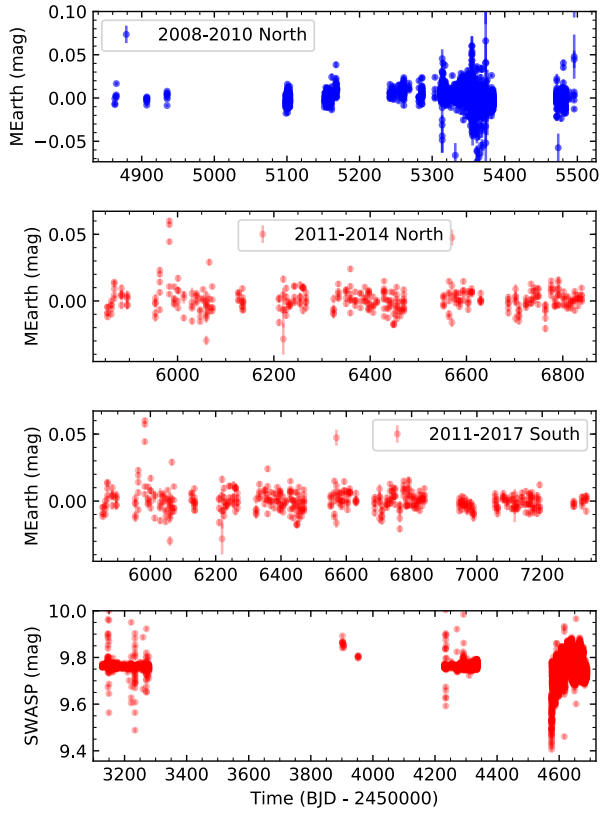

Fig. 2. MEarth and SuperWASP photometric time series for GJ 720 A after 2.5σ clipping applied.

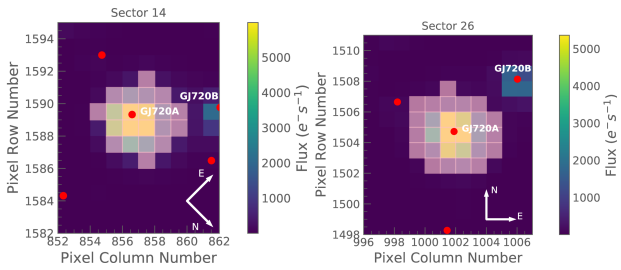

Fig. 3. Target pixel files (TPF) of GJ 720 A (TIC122958010) in *TESS* Sectors 14 and 26. The electron counts are color-coded. The shadowed pixels correspond to the *TESS* optimal photometric aperture used to obtain the simple aperture photometry (SAP) fluxes. The red dots correspond with the bright nearby stars with *TESS* magnitude less than 16. The positions of GJ 720 A and GJ 720 B are indicated.

other source contamination that could affect the transit search. The TPFs files of GJ 720 A with the standard pipeline apertures are shown in Fig. 3. We also included in the figure the bright nearby stars with *TESS* magnitude less than 16. The visual binary companion GJ 720 B is located outside the standard pipeline apertures and therefore we can discard some kind of contaminating flux from it. The light curve files provide simple aperture photometry (SAP) fluxes and photometry corrected for systematics effects (PDC, Smith et al. 2012; Stumpe et al. 2014), being the last ones optimized for *TESS* transit searches.

Table 2. Photometric seasons available for GJ 720 A.

Obs.[a]	Filter/sector	Season	ΔT (d)	N_{obs}	σ
MEarth-North	*RG*715	2008–2010	3,532	632	8.8 mmag
MEarth-North	*RG*715	2011–2014	397	984	6.9 mmag
MEarth-South	*RG*715	2011–2017	536	1,480	6.2 mmag
SuperWASP	...	2004–2008	1,559	12,922	36.7 mmag
EXORAP	*B*	2013–2017	1,479	248	8.6 mmag
APACHE	*V*	2013–2016	1,250	5,900	5.5 mmag
TESS	Sector 14	July 2019	27	18,522	4.8 $\cdot 10^{-4}$ e^-/s
TESS	Sector 26	July 2020	27	16,941	4.8 $\cdot 10^{-4}$ e^-/s

The information regarding the different photometric surveys, the used observing filters/sectors, the number of days covered per observing season, the number of photometric measurements, and the standard deviation of the differential photometry are summarized in Table 2.

4. Analysis of GJ 720 A

4.1. HARPS-N radial velocities, pre-whitening

The first step of the RV data analysis is the identification of significant periodic signals in the time series. The procedure was applied to the full RV data using the Generalized Lomb-Scargle (GLS) periodogram algorithm (Zechmeister & Kürster 2009). We consider significant periods if the power is higher than a chosen false alarm probability (FAP, Zechmeister & Kürster 2009) level of 10% (notable), 1% (prominent), and 0.1%(significant). In Fig. 4 we included the GLS periodograms for the RVs (blue), the spectroscopic activity indicators (green) and the photometry (red) in the frequency range 0.001–0.1 d^{-1} (1000–10 d in time range). The window function of the HARPS-N RV data is depicted in the top panel of Fig. 4 (yellow line). The second panel of Fig. 4 reports the GLS periodogram for the HARPS-N RV dataset. There are several significant peaks higher than the 0.1% FAP located at 19.5 d (light blue shadowed area), ~40 d and ~100 d (purple shadowed areas). The most prominent peak is the one at 19.5 d, that we will consider our most interesting signal from now on.

In what follows, we demonstrate that these three signals are not related to each other by an aliasing effect, which is typically caused by the gaps in the time coverage of the observations (e.g., Dawson & Fabrycky 2010). To identify the presence of possible aliasing phenomena, the spectral window has to be considered. If peaks are seen in the window function, their corresponding aliases will be present in the RV periodograms as $f_{alias} = f_{true} \pm m f_{window}$, where m is an integer, f_{true} is the frequency identified in the RV periodogram and f_{window} the frequency from the window function (Deeming 1975). Typical aliases are those associated with the sidereal year, synodic month, sidereal day, and solar day. There are two significant peaks in the window function at the sidereal 1 and 2 years. Searching for these modulations around the principal peaks of the GLS periodogram of the RV data (19.5, ~40, ~100 d), we found that secondary (lower) peaks around these three values are due to the aliases at 1 and 2 years of the spectral windows (Fig. 5). The three main signals in the RV time series are not related to each other by the observation sampling.

In order to verify whether the 19.5 d signal was coherent over the whole observational time baseline, we produced the stacked Bayesian generalized Lomb-Scargle periodogram (s-BGLS, Mortier et al. 2015) which computes the relative prob-

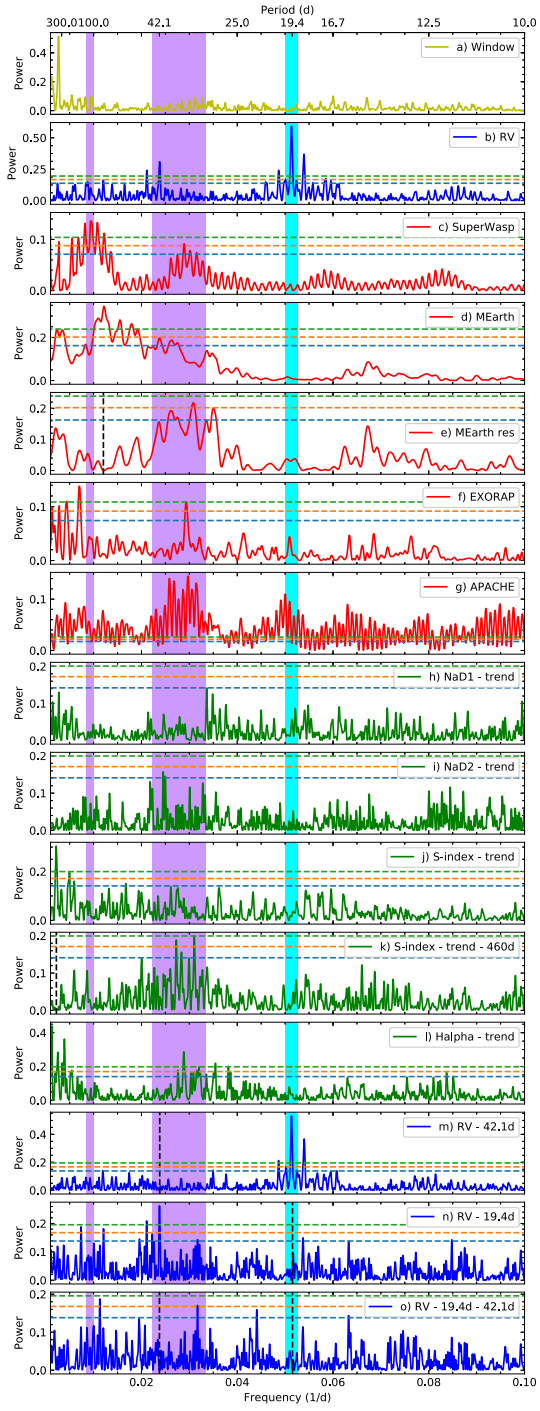

Fig. 4. GLS periodograms for GJ 720 A RV data (blue solid lines), photospheric stellar activity (red solid lines), and spectroscopic stellar activity (green solid lines) in the frequency range 0.001–0.1 d^{-1} (1000–10 d in time range). In all the panels, the horizontal dashed lines indicate FAP levels of 10% (blue), 1% (orange), and 0.1% (green). The shadowed areas indicate the region where the RV highest peaks are found. *a) and b) panels:* Spectral window (yellow line) and HARPS-N RVs (blue line), respectively. *c) panel:* SuperWASP binned photometric data. *d) and e) panels:* MEarth binned photometric data and the residuals after removing the highest peak found at ∼100 d (black vertical dashed line). *f) panel:* EXORAP *B* filter. *g) panel:* APACHE *V* filter binned photometric data. *h) through l) panels:* HARPS-N NaD1, NaD2, Ca II H & K (S-index), and Hα HARPS-N spectroscopic activity indicators with a linear trend removed. *m) panel:* HARPS-N RV residuals after removing the 42.1 d signal, marked with a black vertical dashed line. *n) panel:* HARPS-N RV residuals after removing the planet candidate signal at 19.5 d. *o) panel:* HARPS-N RV residuals after removing the 19.5 and 42.1 d signals. All the activity indicators and the RV data show a significant, broad peak between 35–45 d. This is likely associated with the rotation period of GJ 720 A.

ability between peaks. Figure 6 shows the s-BGLS periodogram of the HARPS-N RV data around 19.5 d and also around the 40 d activity signal. The s-BGLS showed a continuous increasing of the probability at 19.5 d (left panel of Fig. 6) after around 90 observations and thereafter also the signal became narrower, as expected for a Keplerian signal. On the contrary the behaviour of the signal at ∼40 d did not show such high probability and narrow structure. The first maximum of the probability for the ∼40 d signal is produced after around 90 observations and thereafter decreased and increased again for some time. Also exact value of the ∼40 d signal is erratically changing in time, following the increase of the number of observations. This behaviour is typical of an incoherent (in amplitude and phase) signal, as that due to the rotational modulation of a star. The coherence of the 19.5 d period established above does not support its identification as the first harmonic of the ∼40 d period, despite its close value, since it should vary accordingly.

The ∼40 d signal that we could attribute to stellar activity, following the pre-whitening method, can be modeled with a sinusoidal curve of 42.1 ± 0.1 d with a semi-amplitude of 3.02 ± 0.44 m/s in the RV data. After its removal from the HARPS-N RV data (see *m* panel of Figure 4), we found an *rms* of the residuals of 3.36 m/s while the signal at ∼100 d, that we could also relate to stellar activity disappears. The signal at 19.5 d remains in the RV GLS periodogram of the residuals and its significance is still far above the FAP level 0.1%. Now we subtract first the 19.5 d signal (see *n* panel of Figure 4) to observe the behaviour of the ∼40 d signal. The corresponding RV residuals still present the ∼40 d signal with the same GLS power and therefore the same significance. When removing both contributions (19.4 and ∼40 d peaks, see *o* panel of Fig. 4) no additional peaks above a 0.1% FAP are present. Those remaining peaks with 1% and 10% are considered as result of the stellar noise.

4.2. Spectroscopic stellar activity

From the previous section we identified three principal periodic signals (19.5, ∼40, ∼100 d) in the GLS periodogram of the RV data being mandatory the knowledge of their origin. The M dwarfs are on average more active than solar-like stars (Leto et al. 1997; Osten et al. 2005) and therefore the effects of the stellar activity (chromospheric or photospheric) can be confused with planetary signals or even hide them. In order to disentangle the effects of activity from true RV variations we analysed two commonly used chromospheric activity indicators based on measurements of the Hα 6562.82 Å and Ca II H & K 3933.7, 3968.5 Å lines (S-index) and also the sodium doublet (NaD1 and NaD2) provided by TERRA pipeline.

The associated GLS periodograms of all analyzed activity indicators are shown in Fig. 4 (green panels). We also include the FAP levels and the shadowed colored areas that correspond with the principal peaks (19.5, ∼40, ∼100 d) identified from the GLS of the RVs. In particular, the NaD1, NaD2, Hα, and S-index indices present a clear trend in their time-series (green panels of Fig. 1). Analyzing the GLS periodogram we observed this trend as a long-term variability of period > 350 d. For this reason we detrended the NaD1, NaD2, S-index, and Hα time series subtracting a straight line before the analysis of the activity indicators. With the activity indices detrended, all of them present some kind of activity centered around 40 d.

In the Hα case, the ∼40 d signal is also present (FAP level <0.1%) but it is not the highest one. While for the S-index case, after data detrending, the GLS periodogram shows another long-

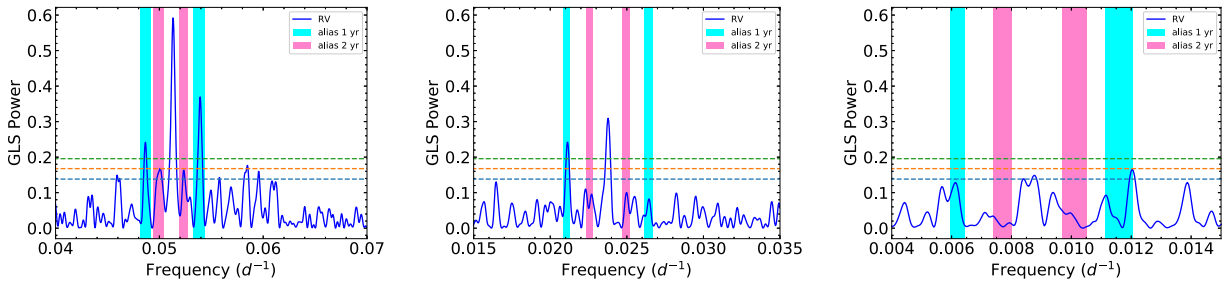

Fig. 5. Zoom-in of the GLS periodogram of the HARPS-N RV data of GJ 720 A (blue solid line) around the strongest signals at 19.5 (*left panel*), 42.1 (*center panel*), and 112.4 days (*right panel*). The corresponding values in the frequency domain are 0.05128, 0.02375, and 0.0890 d^{-1}, respectively. Horizontal dashed lines indicate the different FAPs: 0.1% (green), 1% (orange) and 10% (blue). The 1 and 2-sidereal-year aliases around each of the strongest signals are indicated with cian and purple vertical solid lines, respectively.

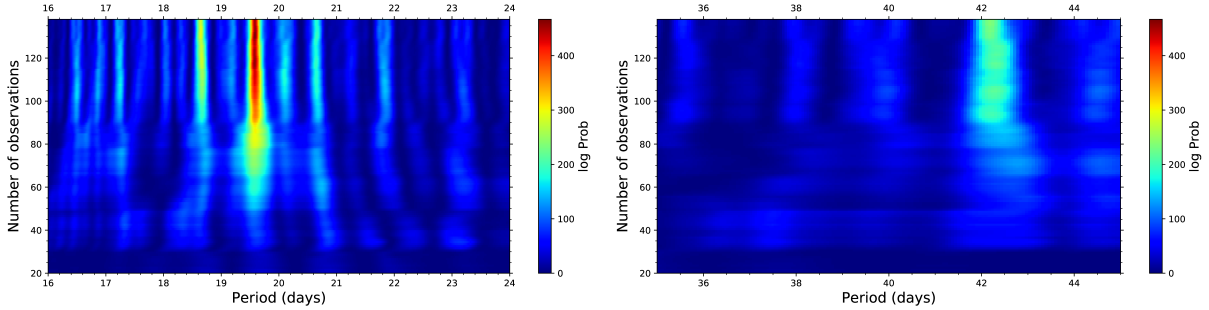

Fig. 6. Evolution of the s-BGLS periodogram of the HARPS-N RV data of GJ 720 A. *Left panel:*The most probable period (the reddest one) at 19.5 days is clearly visible after around $N_{obs} > 80$. *Right panel:* s-BGLS periodogram around 40 d signal produced by the stellar variability.

term variation at 450 d that we also removed (black vertical line in the *k* panel of Fig. 4). After that we obtained a clear, unique, and significant period at 32.21 ± 0.05 days. The same technique was used to obtain the rotation period of the star published by Suárez Mascareño et al. (2018). The authors derived the stellar rotation at $P_{\rm rot}$ = 34.5 ± 4.7 days with the HARPS-N spectra available to date.

Taking advantage of the available 138 HARPS-N RV data points, we modeled the stellar variability of the S-index (original data that include the trend) using a Gaussian process (GP) regression, which is a more sophisticated method than the prewhitening one. The fit was performed using `juliet` (Espinoza et al. 2019) that used `radvel` (Fulton et al. 2018) to model Keplerian RV signals, and `george` (Ambikasaran et al. 2015) to model the stellar variability with GP. We used an exp-sin-squared kernel multiplied by a squared-exponential kernel, which is included as a default kernel within `juliet`. This kernel has the form:

$$k(\tau) = \sigma_{GP}^2 \exp\left(-\alpha_{GP}\tau^2 - \Gamma \sin^2\left(\frac{\pi\tau}{P_{rot}}\right)\right) \quad (1)$$

where σ_{GP} is the amplitude of the GP component given in the same units of the data, Γ is the amplitude of the GP sine-squared component and is dimensionless, α is the inverse squared length-scale of the GP exponential component given in d^{-2}, $P_{\rm rot}$ the period of the GP quasi-periodic component given in d, and τ is the time lag.

All parameters were set with wide priors and in particular the $P_{\rm rot}$ was set free to vary in the range 1–500 d (see Table A.2).

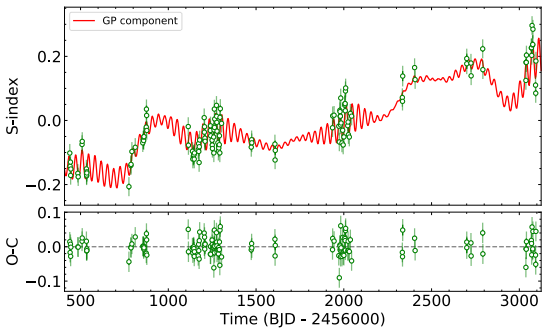

Fig. 7. GJ 720 A original S-index data together with the best model and the residuals. The fitted GP model (red line) corresponds to an exp-sin-squared kernel multiplied with a squared-exponential kernel modeling the stellar variability. The error bars (color green) include the jitter (light green color) taken into account.

The found stellar rotation period, using the GP technique, corresponds with $P_{\rm rot} = 36.05^{+1.39}_{-1.44}$ d with a length-scale median value of 141.28 d (α_{GP}=5.01×10^{-5} d^{-2}). Figure 7 shows the GP model that best fits the S-index data while in Fig. 8 we show the posterior distributions for the GP parameters of the model.

Finally we note that in all the studied chromospheric activity indicators, no significant signals were identified around 19.5 d (light blue colored area in Fig. 4) and therefore the hypothesis of a planet candidate at 19.5 d is now more reliable. All the chromospheric activity indicators show significant peaks in the